Engineer Energy Dissipation in 3D Graphene Nanolattice Via Reversible Snap-Through Instability

Bo Ni
School of Engineering,
Brown University,
Box D, 182 Hope Street,
Providence, RI 02912
e-mail: bo_ni@brown.edu

Huajian Gao[1,2]
Mem. ASME
School of Engineering,
Brown University,
182 Hope Street,
Providence, RI 02912
e-mail: Huajian_Gao@brown.edu

Carbon micro/nanolattice materials, defined as three-dimensional (3D) architected metamaterials made of micro/nanoscale carbon constituents, have demonstrated exceptional mechanical properties, including ultrahigh specific strength, stiffness, and extensive deformability through experiments and simulations. The ductility of these carbon micro/nanolattices is also important for robust performance. In this work, we present a novel design of using reversible snap-through instability to engineer energy dissipation in 3D graphene nanolattices. Inspired by the shell structure of flexible straws, we construct a type of graphene counterpart via topological design and demonstrate its associated snap-through instability through molecular dynamics (MD) simulations. One-dimensional (1D) straw-like carbon nanotube (SCNT) and 3D graphene nanolattices are constructed from a unit cell. These graphene nanolattices possess multiple stable states and are elastically reconfigurable. A theoretical model of the 1D bi-stable element chain is adopted to understand the collective deformation behavior of the nanolattice. Reversible pseudoplastic behavior with a finite hysteresis loop is predicted and further validated via MD. Enhanced by these novel energy dissipation mechanisms, the 3D graphene nanolattice shows good tolerance of crack-like flaws and is predicted to approach a specific energy dissipation of 233 kJ/kg in a loading cycle with no permanent damage (one order higher than the energy absorbed by carbon steel at failure, 16 kJ/kg). This study provides a novel mechanism for 3D carbon nanolattice to dissipate energy with no accumulative damage and improve resistance to fracture, broadening the promising application of 3D carbon in energy absorption and programmable materials. [DOI: 10.1115/1.4045544]

Keywords: constitutive modeling of materials, flow and fracture, micromechanics, structures

Introduction

Carbon micro/nano lattices are a unique family of architected metamaterials constructed from micro/nanoscale carbon constituents [1]. During the past few years, they have demonstrated exciting potentials in reaching theoretical limits of mechanical performances as well as integrating properties which are often mutually exclusive through experimental studies and numerical simulations [2–8]. For example, the glassy carbon nano-honeycomb lattice fabricated through pyrolysis of polymeric microlattice has reached a compressive strength of 1.2 GPa at a density of 0.6 g/cm^3, approaching the lower bound of the theoretical limit set by the bulk glassy carbon [2]. Pyrolytic carbon nanolattices with topologies of octet- or iso-truss have been demonstrated to possess a combination of high specific strength, low density, extensive deformability, and flaw tolerance, which are properties, in general, mutually exclusive in conventional materials [3]. The record-breaking performances of these carbon nanolattices are boosted by at least two factors: the size-dependent properties of the constituents and the well-designed lattice architecture [1]. By reducing the length scale of the components, such as beams or cell walls, to nanoscale, the constituents unlock the properties which are close to their theoretical values. For example, combining theoretical, computational, and experimental studies [9–11], researchers have predicted that the critical size for pyrolytic carbon being flaw tolerant is about ~490 nm [3]. Experimental studies confirm that for carbon nanolattice with a characteristic length (diameters of the struts) below this size, local failure of the constituents becomes flaw insensitive, reaching the theoretical strength of bulk carbon materials [2,3]. The benefit of being small is further coupled with the well-designed lattice architectures, resulting in richer and more balanced combinations of desired properties. For instance, via a systematic computational study of 3D graphene in the topologies of triply periodic minimal surfaces, it has been demonstrated that topology can strongly affect the elastic properties and failure mechanisms of graphene nanolattices [4,5]. In short, the combination of small-scale carbon constituents and unlimited architecture designs of lattice opens a broad exploration space for better material properties in carbon nanolattices.

Besides pursuing high specific strength, ductility is also particularly important to carbon nanolattices for robust performances [7]. At the material level, the carbon constituents are intrinsically brittle. Including bulk glassy carbon [2,6], the basic material building block of most carbon nanolattices is graphene, a two-dimensional (2D) atomically thin layer of carbon atoms connected by sp^2 hybrid covalent bonding [12]. As one of the strongest known materials, graphene has a theoretical strength of 130 GPa [13] (two orders larger than that of bulk glassy carbon, 2~3 GPa [2]). However, experimental studies have unveiled that the fracture toughness of graphene is only 16 J/m^2 [14], which is close to that of an ideally brittle solid [15]. As the characteristic length of carbon nanolattices falls smaller to make use of the ultrahigh

[1]Corresponding author.
[2]Present address: School of Mechanical and Aerospace Engineering, College of Engineering, Nanyang Technological University, 70 Nanyang Drive, Singapore 639798, Singapore.

Manuscript received October 30, 2019; final manuscript received November 24, 2019; published online November 26, 2019. Assoc. Editor: Yonggang Huang.

strength of graphene, it is also important to enhance the toughness and ductility of the nanolattices. At the structure level, buckling is an important mechanism to dissipate energy in nanolattice materials under compression [16–18]. However, permanent and continuous damage often accompanies buckling events. For example, it is observed that for hollow metallic and ceramic microlattices, the hysteresis loops of stress–strain curves shrink as the number of loading cycles increases, especially over the first few cycles [18,19]. Also, while being accessible under compression [20,21], buckling can have a much limited effect on energy dissipation under tensile loading. For instance, molecular dynamics (MD) simulations have demonstrated that under tension, graphene nanolattices, such as graphene gyroids, dissipate energy mainly through crack nucleation and propagation, which accumulate permanent damage and degrade the material systems [4,5]. Given the great potentials of carbon nanomaterials, it is important to enrich the design library of carbon nanolattices with examples of novel energy dissipation mechanisms in order to overcome this challenge.

Like buckling, snap-through instability has been a long-time research topic [22–29]. Recent studies unveil some unique advantages of this instability. On one hand, at macroscale, by carefully designing and arranging the snap-through units in metamaterials, sequential snap-through instabilities can be triggered under not only compressive but also tensile loading conditions [25,28]. Cyclic loading tests demonstrate that these built-in instabilities suffer little irreversible damage [28]. Metamaterials with snap-through instability often exhibit multiple mechanically stable states, which open doors to the design of shape-reconfigurable materials [25]. On the other hand, at small scales, basic conceptual units with mechanically bi-stable states and snap-through instability [30–33] have been adopted to explain deformation behaviors of phase transforming materials, including structure proteins with compactly folded or unfolded domains [34,35] and shape memory alloys undergoing martensitic phase transformation [36]. Such a universal structure-to-property relationship indicates great potential in engineering complex overall deformation behavior via bi-stable units and snap-through instabilities.

The present study is aimed to address the challenge of toughening carbon nanolattice with the potential of snap-through instability in engineering overall material behavior. Through mechanism-inspired structure design, MD simulations, and theoretical analysis, we present a novel design of 3D graphene nanolattice with snap-through instability and demonstrate that it can effectively dissipate deformation energy without accumulating irreversible damages via pseudo plastic deformation.

Unit Cell Design

We choose 2D graphene as a basis for our nanolattice design due to its outstanding mechanical properties. To adapt to the 2D geometry of graphene, we focus on shell-based designs.

At macroscale, numerous applications and studies have presented various examples of shell structures with snap-through instabilities [37–42]. Here, we borrowed inspiration from one of the simplest cases, the flexible straw [43,44], which can change length by transforming between the folded state and the extended state (Figs. 1(*b*) and 1(*c*)). As shown in Fig. 1(*a*), the unit cell structure of such a flexible straw is a pair of intersecting conical frustra (the outer frustum, Q-T-P and the inner one, Q-P, intersecting at the folds P and Q). By designing the geometrical parameters of the unit cell, a recent study [45] has demonstrated that both the axially folded state and the extended state can be mechanically stable (Figs. 1(*b*) and 1(*c*)) for elastic shells. Here, we constructed a full-atom model of the graphene counterpart to such a unit cell by taking advantage of the methodology of topological design [46–48]. As shown in Fig. 1(*d*), phase field crystal modeling [49–51] was adopted to simulate the growth of the 2D crystal on the designed geometry of the conical frustra. The thermal stability of the obtained crystal structure was validated by relaxing it under an NPT ensemble with a Nose-Hoover thermostat

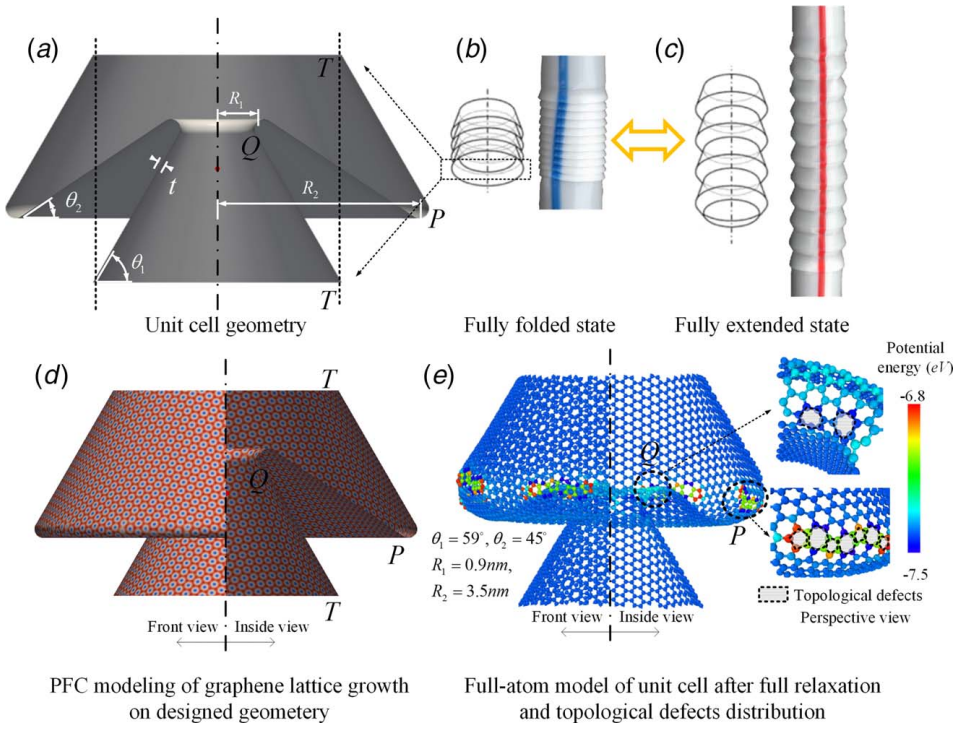

Fig. 1 Unit cell of the shell structure in flexible straws and its nanoscale graphene counterpart engineered via topological design. (*a*) Geometry of the unit cell structure in straws. (*b*) and (*c*) The fully folded and fully extended states of flexible straws. (*d*) Phase field crystal (PFC) simulation of a 2D crystal sample growing on the designed shell surface. (e) The atomic structure of the graphene unit cell with straw-like geometry after MD relaxation and the topological defects distributed at the inner and outer folds.

[52] at 0 Pa and 300 K for 50 ps using MD (details of MD simulations can be found in the Appendix). The dimensions of the relaxed sample are listed in Fig. 1(*e*). It should be noted that even through the relaxed model does not fully conform to the designed geometry (Fig. 1(*d*)), the straw-like topology is stably maintained (Fig. 1(*e*)). Further inspection showed that topological defects [46,53], such as disclinations and dislocations, only concentrate at the connections of the two frustra, accommodating and stabilizing the curvature transition (Fig. 1(*e*)). The inevitable presence of topological defects, their residual stress [47] as well as the Van der Waals (VdW) interactions [54] between graphene frustra make the atomic sample different from its counterpart at large scale.

To explore the snap-through instability and possible mechanically stable states of such straw-like unit cells, uniaxial tension tests were performed by applying a constant strain rate of 10^8/s to the simulation box along the axial direction. During the test, a periodic boundary condition was applied along the axial direction and an NVT ensemble with a Nose-Hoover thermostat [52] was adopted to maintain a constant temperature of 10 K. The force–strain and potential energy–strain curves are shown in Fig. 2(*a*). The potential energy curve shows two parabolic-like parts centered around the folded state (State A) and the extended state (State D), indicating both states have positive stiffness. Relaxation and loading tests via MD demonstrated they are mechanically stable. In the transition region, the force–strain curve suffers a non-positive derivative, resulting from the snap-through instability and the corresponding negative incremental stiffness. Through the snap-through instability, the unit cell achieves a 33% elongation without any irreversible damage to the crystal structure (Fig. 2(*b*)). Careful inspection showed that the snap-through event mainly takes place at the inner frustum (P-Q in Fig. 2(*b*)) with the outer frustum (Q-T-P in Fig. 2(*b*)) serving as a constraint to its deformation. At the folded state, the inner frustum is already self-stressed under no external loading (Fig. 2(*c*)). As the external tension increases, the highly compressive stress state is pushed toward the inner fold, Q (Fig. 2(*d*)). At the critical moment, the axial symmetry of the deformation is broken (Fig. 2(*e*)) and the inner frustrum flips out (Fig. 2(*f*)), resulting in a snap-through event (Fig. 2(*g*)). Compared to the folded state (Fig. 2(*c*)), the residual stress in the inner frustrum is reduced in the extended state (Fig. 2(*f*)). Correspondingly, the potential energy in the extended state is lower than that of the folded state (Fig. 2(*a*)) even through the two share the same atomic topology. In short, the straw-like unit cell possesses two mechanically stable states and can snap-through between them under tension, suffering no permanent damage. It is also interesting to note that similar bi-stable states and snap-through events have been studied in shell systems at macroscale. For example, via experiments and finite element simulations, mirror buckling and snap-through events in spherical cap shells have been studied, where it is demonstrated that the initial asymmetrical buckling can make the snap-through more robust [41]. Recently, an energy landscape analysis is conducted for cylindrical shells. Such a detailed energy landscape has proved to be an insightful guidance for designing controllable buckling paths between different states [42]. Inspired by these advances in shell buckling study, we wish to point out that it is very likely the straw-like unit cell presented here can be further tuned for more optimized mechanical behavior. For instance, by adjusting its geometrical dimensions, defect/imperfection distributions and residual stress fields, the unit cell may demonstrate a higher stress level for snap-through transition and a larger

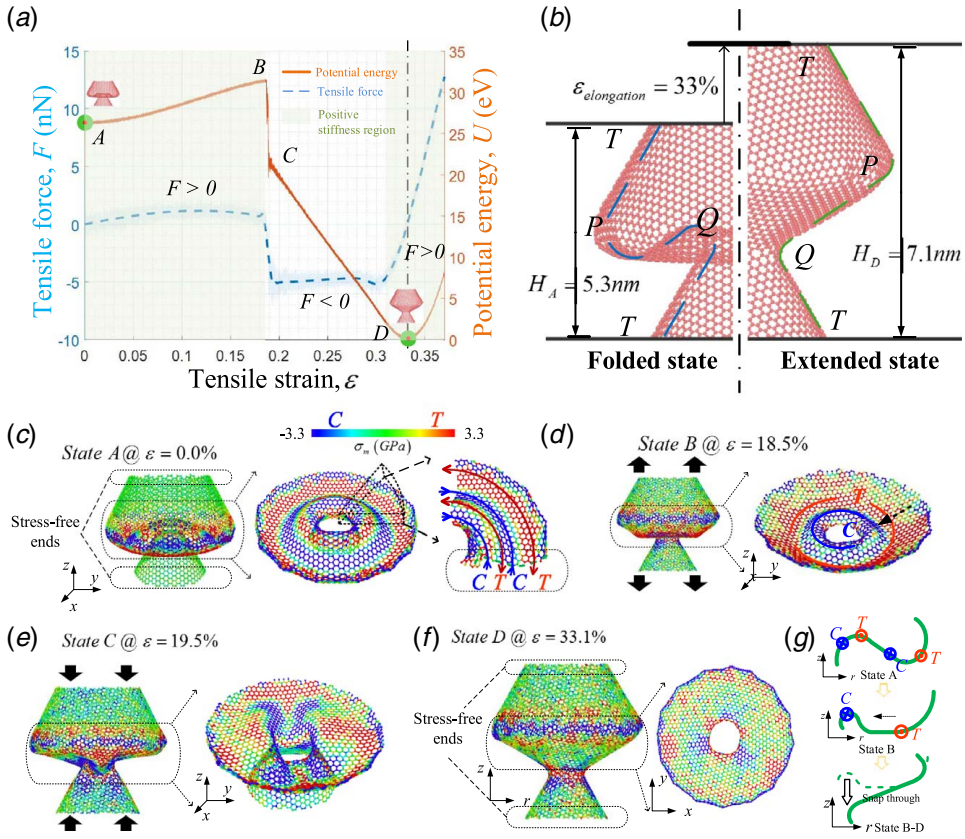

Fig. 2 The two stress-free stable configurations of the unit cell and the process of a snap-through event. (*a*) The force–strain and potential energy–strain curves of the unit cell transforming from the folded state to the extended state. (*b*) Geometry of the two loading-free equilibrium configurations of the unit cell. The two halves of the unit cell are in the folded and extended states, respectively. (*c*)–(*f*) Snapshots of a snap-through event during a tension test in MD simulation. (*g*) 2D sketch of the deformation process of the inner frustrum during the snap-through process.

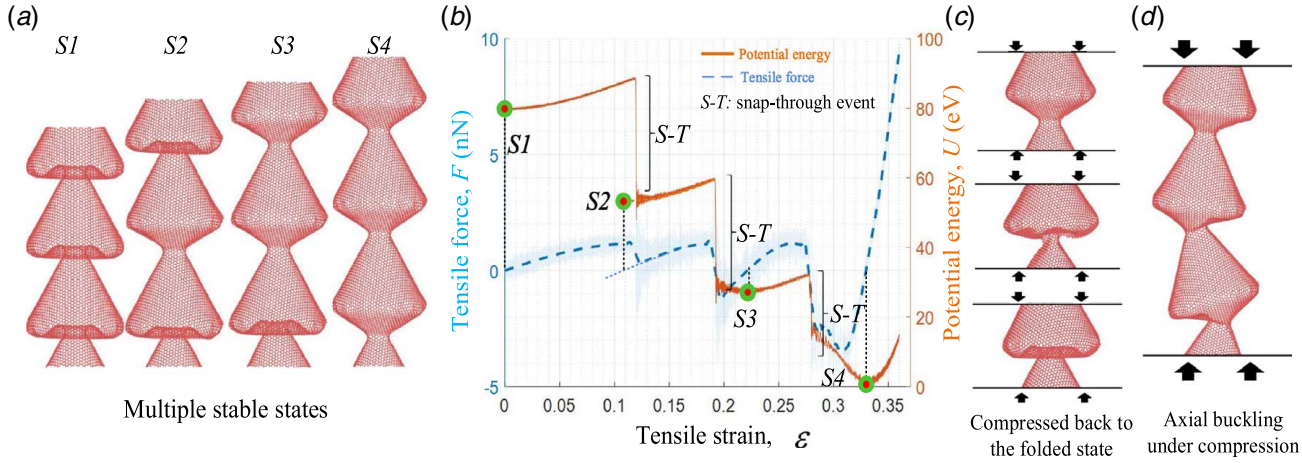

Fig. 3 1D lattice design: a straw-like CNT. (*a*) The four stress-free equilibrium configurations with different lengths. (*b*) Force–strain and potential energy–strain curves during transition from the fully folded stated to the fully extended state under tension via MD. (*c*) One unit cell compressed back to its folded state without suffering axial buckling. (*d*) Axial buckling of the SCNT with three unit cells under compression.

elongation between the folded and the extended states. We leave this optimization to a future study and focus on the coupling between the unit cell behavior and the lattice-level design in the current study.

In the following section, we combine the unit cell with different lattice designs to construct 1D and 3D graphene nanolattices and study their collective deformation behaviors, aiming at engineering effective energy dissipation by leveraging the effect of the snap-through instability.

Lattice Design: 1D and 3D Cases

Straightforwardly, by repeating the unit cell along the axial direction, we obtain the 1D lattice of a straw-like CNT (SCNT). Because each unit cell within the SCNT can choose either the folded state or the extended state, the SCNT sample can have multiple mechanically stable states. Under tensile loading along the axial direction, the SCNT can transform through these states and achieve different axial lengths, making it a reconfigurable 1D nanolattice. We validated this capability via MD simulations. One example SCNT with three unit cells is transformed from the fully folded configuration to the fully extended state under tensile loading in MD (Movie M1).[3] As shown in Fig. 3, four different equilibrium lengths are identified from MD (Fig. 3(*a*)). During the tensile loading process, they are separated by discrete snap-through events of individual unit cells (Fig. 3(*b*)). At each instability event, the stored strain energy (solid line in Fig. 3(*b*)) is partially released and dissipated into the environment via thermal vibrations. Correspondingly, the loading force drops, leaving a saw-teeth like force–strain curve (dash line in Fig. 3(*b*)).

One limitation for this 1D nanolattice of SCNT is that it can be hard to transform the extended configuration back to the folded one due to global axial buckling of SCNT under compression. As shown in Figs. 3(*c*) and 3(*d*), under compression, even though the straw-like unit cell can snap back to the folded state, the SCNT with three unit cells buckles along the axial direction before the backward snap-through can happen. This asymmetry in tension and compression limits the reconfigurability of 1D SCNT in cyclic loading. Next, we construct a 3D lattice to overcome this limitation.

As shown in Fig. 4(*a*), parallel 1D SCNTs are assembled into a bundle-like architecture according to a square lattice with a lattice parameter, a, forming a new 3D graphene nanolattice. We chose a to be smaller than the outer diameter the SCNTs, $2R_2$ (Fig. 1(*a*)), so that the neighboring SCNTs are interconnected through covalent bonding. We designed the atomic structure using topological design [46]. As shown in Fig. 4(*b*), topological defects appear and help to accommodate the curvature transition at the connections. To investigate the deformation behavior of such 3D graphene nanolattices, we performed tension–compression cyclic loading along the vertical directions (which is the axial direction of the SCNTs) using MD. It is demonstrated that these 3D graphene nanolattices can snap forward and backward between the fully folded and extended states under cyclic loading without suffering global buckling or irreversible damage (see Movie M2 and M3 for details),[4] which makes them elastically reconfigurable.

It should be noted that the number of unit cells along the axial direction can affect the deformation behavior of the 3D graphene nanolattices. In a reference case of one single unit cell under cyclic loading along the axial direction (Figs. 4(*c*) and 4(*d*)), it is observed that the mechanical responses along tension and compression paths show very limited differences. For example, in Figs. 4(*c*) and 4(*d*), the stress–strain and strain energy density–strain curves of tension and compression tests are close to each other. Correspondingly, very limited energy can be dissipated during such a displacement-controlled loading loop. However, the energy dissipation is amplified when there is more than one unit cell along the axial direction. For instance, in Figs. 4(*e*) and 4(*f*), a sample with 3-by-3-by-3 unit cells is tested under the same loading condition (Movie M2 and M3).[5] The stress–strain history takes different paths under tension and compression. Correspondingly, a hysteresis loop appears, and the energy associated with it is dissipated after the cycle (Fig. 4(*e*)). Intuitively, this hysteresis behavior can be related to the snap-through instability. As shown in Figs. 4(*e*) and 4(*f*), the snap-through events correspond to the sudden jumps in the stress–strain and strain energy–density curves. Two observations can be made here. First, the pairs of neighboring snap-through events from tension and compression paths (such as S$-T$ i and S$-T$ (7 $-i$), where $i = 1, 2, 3$, in Figs. 4(*e*) and 4(*f*)) happen at different strain values. Second, in the regions with a strain value between one pair of such snap-through events, the strain energy density curves along tension and compression paths deviate from each other (Fig. 4(*f*), regions with dash line arrows), indicating that the system can be in/near configurations with different equilibrium lengths and stiffnesses. To systematically explain the relationship between the hysteresis behavior, snap-through instability, and

[3]https://bo-ni.github.io/snapping-3D-graphene/videos/

[4]See Note 3.

[5]See Note 3.

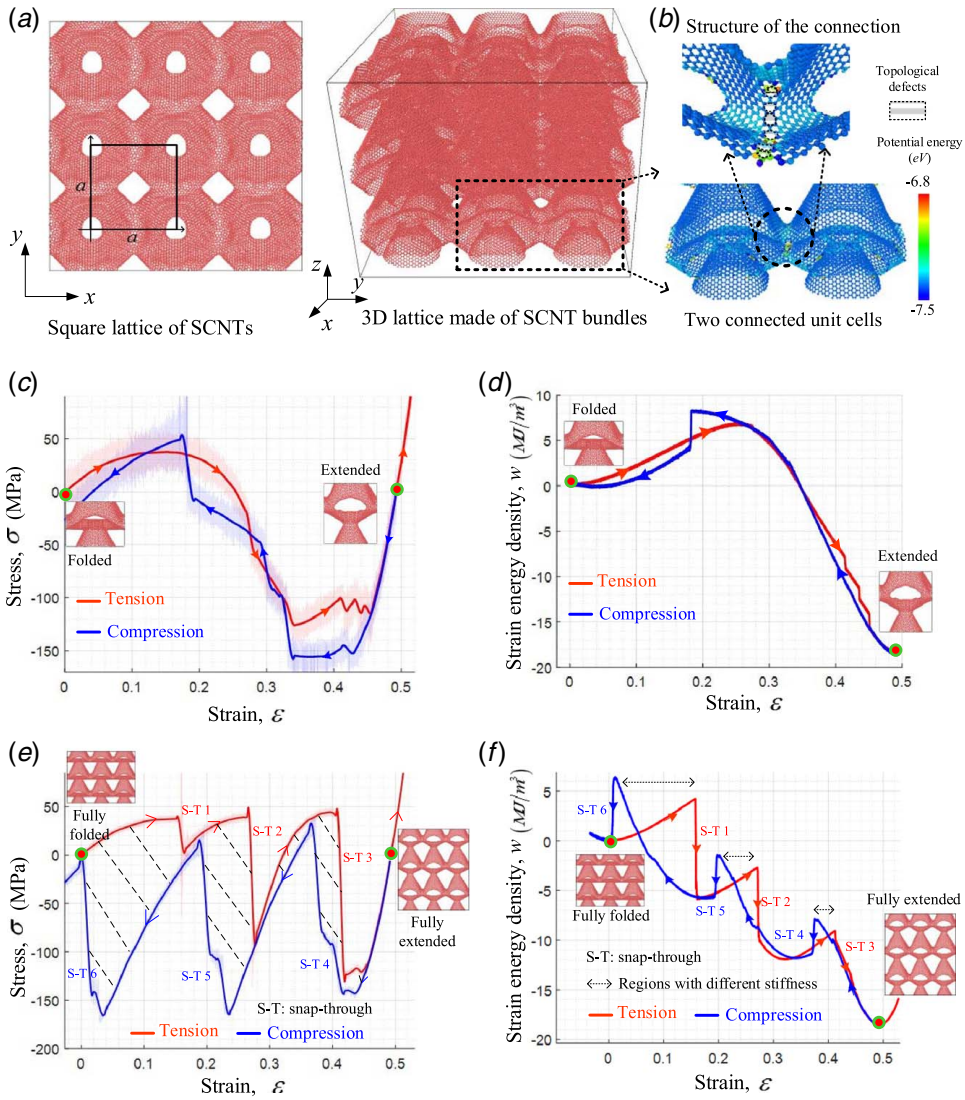

Fig. 4 3D design: 3D graphene nanolattice made of straw-like graphene unit cells. (*a*) The square lattice structure of SCNT bundles. (*b*) The covalently bonded connection between neighboring unit cells and the topological defect distribution nearby. (*c*) and (*d*) The stress–strain and strain energy density–strain curves of a single unit cell under a tension–compression loop between the folded and extended states. (*e*)–(*f*) The stress–strain and strain energy density–strain curves of a 3D graphene nanolattice with 3-by-3-by-3 unit cells under a tension–compression loop between the folded and extended states.

multi-stable configurations, a theoretical model is developed in the next section.

Theoretical Model

In this section, we constructed a theoretical model to explain our observation of 3D graphene nanolattice with snap-through stability and predicted the collective behavior of samples with large members of unit cells.

Phenomenologically, our 3D graphene nanolattice can be modeled as a series of identical unit cells connected one after another along the axial direction. For each unit cell, there exits two equilibrium configurations with different lengths and stiffnesses. Correspondingly, we adopted a theoretical model of 1D chain of bi-stable elements to study the nanolattices (Fig. 5(*a*)). Similar models have been successfully applied to understand the rate independent hysteresis of phase transforming materials [30,31,55], protein deformation [56,57], and deformation behavior of polymeric foams and carbon nanotube foams [58].

First, the deformation behavior of the unit cell of our 3D graphene nanolattice is represented by a bi-stable elastic element. Based on our MD results (Figs. 4(*c*) and 4(*d*)), the deformation of the unit cell under both tension and compression can be represented by a single stress–strain curve with no hysteresis loop (Fig. 5(*b*)), $\sigma = \sigma_{bi}(\varepsilon)$. Accordingly, the tangential stiffness E_t, defined as $E_t = \sigma'_{bi}(\varepsilon) = \partial\sigma/\partial\varepsilon$, varies, where σ and ε are the stress and strain along the axial direction of the unit cell. Based on the sign of tangential stiffness, there exist two stable phases with $E_t > 0$, namely Phase I for $\varepsilon < \varepsilon_I^T$ and Phase II for $\varepsilon > \varepsilon_{II}^C$, separated by a spinodal region with $E_t < 0$, where ε_I^T and ε_{II}^C are strain values reaching zero tangential stiffness, i.e., $\sigma'_{bi}(\varepsilon_I^T) = \sigma'_{bi}(\varepsilon_{II}^C) = 0$. The presence of this spinodal region breaks down the one-to-one mapping between stress and strain for $\sigma \in (\sigma^C, \sigma^T)$ and $\varepsilon \in (\varepsilon_I^C, \varepsilon_{II}^T)$, where σ^C and σ^T are the lower and upper bounds of stress in the spinodal region, $\sigma^C = \sigma_{bi}(\varepsilon_{II}^C)$, $\sigma^T = \sigma_{bi}(\varepsilon_I^T)$, ε_I^C and ε_{II}^T satisfy $\sigma_{bi}(\varepsilon_I^C) = \sigma^C$ in Phase I and $\sigma_{bi}(\varepsilon_{II}^T) = \sigma^T$ in Phase II (Fig. 5(*b*)). For our specific unit cell with $\sigma^C < 0 < \sigma^T$, there are

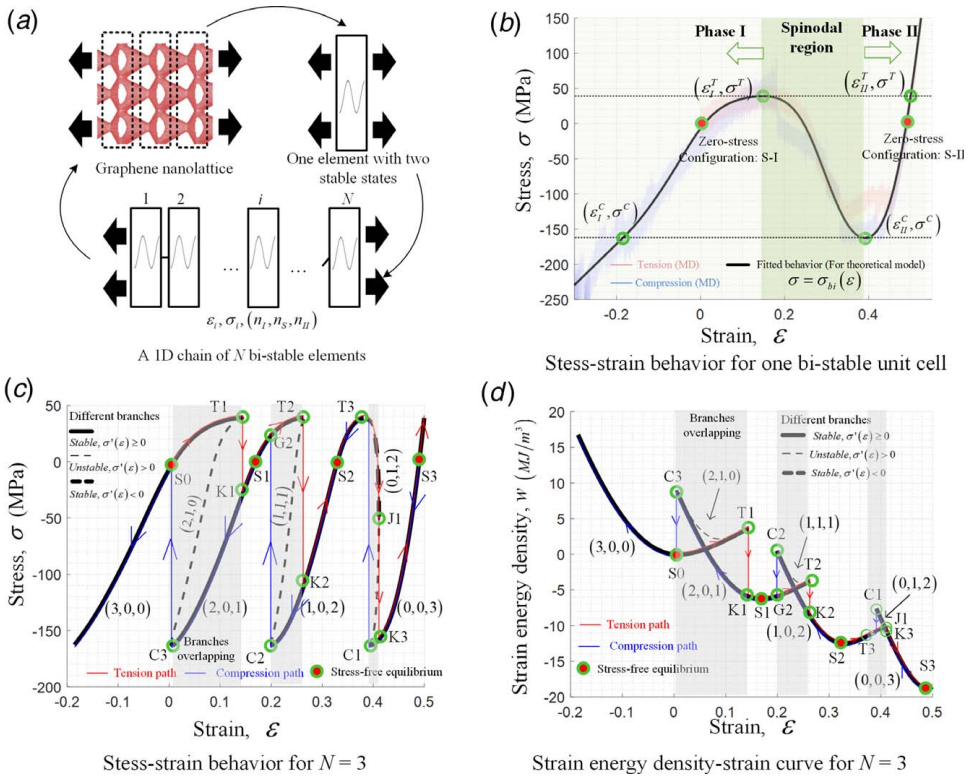

Fig. 5 A theorical model of the 1D chain of bi-stable elements. (*a*) Abstracting the graphene nanolattice with a straw-like unit cell into a 1D bi-stable element chain. (*b*) The constitutive law of a single bi-stable element based on the MD data. (*c*) and (*d*) Theoretical predictions of the stable deformation branches and the paths taken under tension and compression loading on the stress–strain and strain energy density–strain curves.

three stress-free equilibrium configurations ($\sigma = 0$). The one in the spinodal region is not mechanically stable while those two in Phase I and Phase II are, which makes our unit cell a bi-stable elastic element defined by a single stress–strain curve as shown in Fig. 5(*b*).

Second, consider the static/quasi-static deformation of the 1D chain of $N \geq 2$ such bi-stable elements connected in series. In equilibrium, the strain of the chain, $\bar{\varepsilon}$, is the average over all elements and the stress of chain, $\bar{\sigma}$, is continuous through all members

$$\bar{\varepsilon} = \frac{1}{N}\sum_{i=1}^{N} \varepsilon_i \qquad \bar{\sigma} = \sigma_i, \quad i = 1, 2, \ldots, N \tag{1}$$

where ε_i and σ_i are strain and stress of the ith element in the chain. Combining Eq. (1) with the constitutive relation of the individual element

$$\sigma_i = \sigma_{bi}(\varepsilon_i), \quad i = 1, 2, \ldots, N \tag{2}$$

as depicted numerically in Fig. 5(*b*), all possible equilibrium configurations can be found for a given $\bar{\sigma}$ or $\bar{\varepsilon}$. However, it should be noted that the available equilibrium configurations are not necessarily stable. Here, we are only interested in those which are mechanically stable to be physically meaningful (and relevant to MD simulations at finite temperature). The multiple equilibrium configurations can be distinguished by the state of the system, i.e., the numbers of elements in the three phases, (n_I, n_S, n_{II}), where n_I, n_{II}, and n_S are numbers of elements in Phase I, II, and the spinodal region, respectively, $n_I + n_{II} + n_S = N$. Previous studies on similar bi-stable element chains [30,59] have shown that the equilibrium configuration is mechanically stable only if

$$n_S = 0 \quad \text{or} \quad \begin{cases} n_S = 1 \\ \dfrac{\partial \bar{\sigma}}{\partial \bar{\varepsilon}} < 0 \end{cases} \tag{3}$$

i.e., the equilibrium configurations with no element in the spinodal region, $n_S = 0$, are stable; for system with only one element in the spinodal region, $n_S = 1$, it is stable only if the overall tangential stiffness is negative. Combining this criterion with the constitute law of individual bi-stable elements, Eq. (2) and the constraint of the 1D chain, Eq. (1), we can obtain the stable branches of deformation behavior of the 1D chain under all possible system states, (n_I, n_S, n_{II}). One example of these branches in stress–strain and strain energy density–strain curves is shown in Figs. 5(*c*) and 5(*d*) (black solid lines and thick dash lines) for a chain of $N = 3$. There exist $N + 1$ branches for system states with $n_S = 0$, i.e., $(N - i, 0, i)$, $i = 0, 1, \ldots, N$ (black solid lines in Figs. 5(*c*) and 5(*d*)). They all have a convex shape in strain energy density curves (Fig. 5(*d*)) with one local minimal ($Si, i = 0, 1, \ldots, N$), indicating positive stiffnesses and stress-free equilibrium configurations. They are terminated at the points (Ti, Ci, $i = 1, 2, \ldots, N$) where the stress reaches the critical values (σ^T or σ^C) to push one of their elements into the spinodal region. Interestingly, these termination points make the $N + 1$ branches overlap with each other over finite strain intervals. These $N + 1$ stable branches are connected by another N branches for system state with $n_S = 1$ (black dash lines in Figs. 5(*c*) and 5(*d*)), forming a connected path. However, for our graphene nanolattice case, except for a small portion, T3-J1 (thick dash line), most parts of the N branches with $n_S = 1$ have a positive tangential stiffness and are therefore not stable. Consequently, the available stable branches (S0-T1, C3-S1-T2, C2-S2-T3-J1, C1-S3 in Figs. 5(*c*) and 5(*d*)) between the fully folded and extended states (S0-S3) are

disconnected fragments with strain overlapping in stress–strain and strain energy density–strain curves.

It is the discontinuity and overlapping of the stable deformation branches that distinguish the collective behavior of elements in the 1D chain from that of one element in monotonical and cyclic loading. First, consider a monotonically increasing tensile loading applied to the chain of three elements in a displacement-controlled way (S0-T1-K1-T2-K2-J1-K3-S3 in Figs. 5(*c*) and 5(*d*)). Starting from the fully folded state, S0, in the branch of (N, 0, 0), the system raises the stress and accumulates energy until reaching the end of this branch, T1 with a stress of σ^T. The continuity of the overall strain required by the displacement-controlled loading condition can be used to find the next stable deformation branch. Accordingly, in a discrete manner, the system has to switch to the next available branch, ($N-1$, 0, 1), at the point of the same strain via a snap-through event. Assuming the system is overdamped, this sudden change of system state results in a drop in the stress response and partially releases the energy of the system, which is not observed in the case of the one bi-stable element. Similar changes of system state reappear at the right end of the each stable branches until the fully extended state, *SN*, on the last branch (0, 0, N) is reached, leaving behind a saw-teeth like stress–strain curve. During this loading path, the dissipated energy includes not only the work done by the external loading but also the energy difference between the stress-free configurations, *SN* and *S*0. Second, consider a full loop of tension–compression loading. Like in the tension path, the saw-teeth stress–strain curve and sudden drops in system energy also appear at the left end of each stable branch (*Ci*, $i=1, 2, 3, \ldots$ in Figs. 5(*c*) and 5(*d*)) along the compression path from *SN* to *S*0. Moreover, due to the overlapping of different stable deformation branches in strain intervals, the system can choose among different stable branches under tension and compression over the same strain interval. Correspondingly, over these intervals the system has different states, showing different stiffness, stress, and strain energy responses (shaded regions in Figs. 5(*c*) and 5(*d*)). The separation of loading paths in tension and compression results in hysteresis loops under cyclic loading, which is also absent in the single element case. After a full loop, the system can fully recover with no energy change. The nontrivial work done by the external loading is fully dissipated through the hysteresis loops between tension and compression paths in the stress–strain curve. In summary, the theoretical model predicts that the collective behavior of bi-stable elements in a 1D chain gives birth to the discontinuity and overlapping of stable deformation branches. The switching between different branches results in saw-teeth stress–strain curves under monotonical loading. The different choice of the overlapped branches yields the hysteresis loops in cyclic loading. These predictions explain the behaviors observed in MD simulations (Figs. 4(*e*) and 4(*f*)).

Pseudoplastic Behavior in Graphene Nanolattices With Large Numbers of Unit Cells

To quantitatively validate the theoretical model, we compare its prediction to the results of MD simulations. A tension–compression test was applied to a 3D graphene nanolattice with 3-by-3-by-10 unit cells using MD (Movie M4 and M5).[6] Its result is compared with the prediction of the theorical model for the case of $N=10$. It should be noted that there exist some important differences between the assumptions of the theoretical model and the MD simulation conditions. In the theoretical model, it is assumed that the system is overdamped, and the deformation is quasi-static (i.e., no kinetic effect has been included) and the strain rate is infinitely low. In contrast, the MD simulations are performed with a constant temperature of 10 K and a relatively high strain rate of 10^8/s. Under such a simulation condition with kinetic effects, the snap-through events can be triggered earlier; several unit cells may snap at the same time. After snap-through events, the suddenly released deformation energy may excite extra fluctuations and it takes time for the associated thermal energy to be absorbed by the environment (see Movies M4 and M5).[7] In spite of these differences, as shown in Figs. 6(*a*) and 6(*b*), the history of stress and strain energy density during the full loading cycle still shows a reasonably good agreement between MD results and theoretical predictions. This consistency indicates that the deformation behavior of the graphene nanolattice in this study is not sensitive to strain rate and can be well captured by both MD and the theoretical model.

Comparing the MD results of cases for $N=3$ (Figs. 4(*e*) and 4(*f*)) and $N=10$ (Figs. 6(*a*) and 6(*b*)), it is also noted that as the number of the unit cell along the axial direction increases, the amplitude of stress oscillations along tension/compression paths decreases and the area of hysteresis loop increases. Based on this observation, it becomes interesting to predict the asymptotic behavior of nanolattice samples with large numbers of unit cells and ask what is the upper bound of energy dissipation for this nanolattice design. While the full-atom MD simulations may be limited by the available computational power, the efficient theoretical model developed above is suitable for this task.

By continuously increasing N (from 10 to 1000) in the theoretical model, we observed that the deformation behavior converges to a pseudoplastic behavior with a finite hysteresis loop. For stress level between σ^C and σ^T, as N increases, the available stable deformation branches (gray lines in Figs. 6(*c*) and 6(*d*) for $N=1000$) increases and become densely packed between the fully folded and extended configurations. The distances between neighboring branches become smaller and the overlapping regions become larger. Correspondingly, the amplitude of stress drops due to switching between two neighboring branches decreases and averaged stress levels approach ending points of the stable branches, which are σ^C or σ^T. The plasticity-like behavior with flow stress σ^C and σ^T in tension and compression, respectively, is observed (K-L and M-N in Fig. 6(*c*)). However, there is no irreversible damage accumulated in this reconfigurable nanolattice during the process. So, we term this as a pseudoplastic behavior. The hysteresis loop formed by these two stress plateaus is finite because the branch overlapping only exists over the strain interval, (ε_I^C, ε_{II}^T). The left and right boundaries of this hysteresis loop are confined by the stress–strain curve of the constituent bi-stable element between σ^C and σ^T in Phase I and Phase II, respectively (K-N and M-L in Fig. 6(*c*)). For stress level beyond the interval (σ^C, σ^T) or strain level beyond (ε_I^C, ε_{II}^T), the only stable states are (N, 0, 0) or (0, 0, N) and the nanolattice behaves in the same way as one unit cell does.

It is interesting to note that the overall behavior of such a nanolattice with a large number of unit cells is different from but strongly connected to that of its constituent element. It is the lattice arrangement that enables the novel deformation behavior in the assembly level, such as pseudoplasticity and hysteresis. At the same time, the deformation behavior of the single bi-stable element determines the bounds of the pseudoplasticity and hysteresis loops at the lattice level. The strong connection between the behavior of the overall lattice and its constituent provides a promising way to preserve superior properties of nanoscale constituent up to the lattice scale. For example, the reversible snap-through capability of the specific straw-like unit cell studied in the present work benefits from the ultrahigh strength, in-plane stiffness [13], and outstanding bending flexibility [60] of graphene. With a density of 453 kg/m^3 (in the fully folded state), the graphene nanolattice made of such unit cells is predicted to have flow stresses of 39 MPa in tension and −163 MPa in compression over a strain ranging between −0.18 and 0.49. The energy dissipation per unit mass for a full loop between the fully folded and extended states can approach 233 kJ/kg, and this process is

[6]See Note 3.

[7]See Note 3.

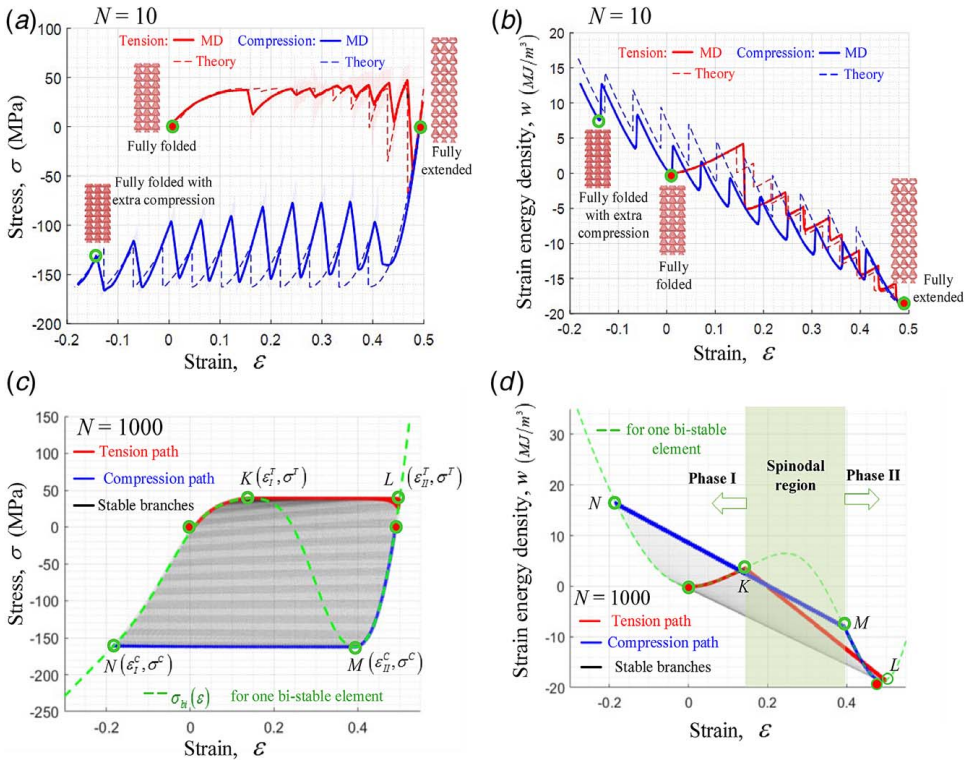

Fig. 6 Validating the theoretical model and predicting the collective behavior of nanolattice with a large number of unit cells. (*a*) and (*b*) MD results and theoretical predictions of stress–strain and strain energy density–strain curves of the nanolattice with ten elements along the axial direction during a tension–compression loop. (*c*) and (*d*) Theorical prediction of the deformation of a nanolattice with 1000 elements along the axial direction and its comparison to that of a single bi-stable element.

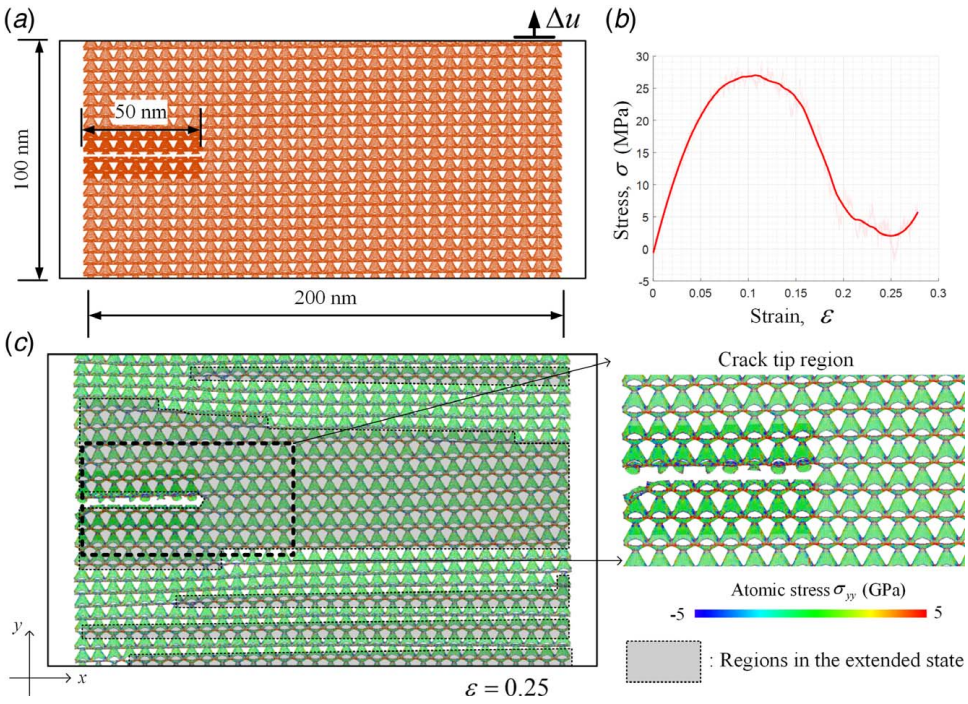

Fig. 7 MD simulation of a tension test of a graphene nanolattice slab with an edge crack. (*a*) Geometry of the graphene nanolattice. (*b*) The overall stress–strain curve. (*c*) Crack trapping due to the band-like region around the crack tip transformed into the extended state via snap-through events.

purely elastic with no permanent damage. Optimization of the geometry and topological defect distribution of the unit cell may further improve this specific energy dissipation density of the nanolattice. Meanwhile, for carbon steel SAE 1020 annealed, with a density of 7872 kg/m^3 and a toughness of 128, 755 kJ/m^3, the energy absorption per unit mass at failure is 16.4 kJ/kg, which is one order of magnitude smaller than the predicted value of the graphene nanolattice studied here.

At last, we demonstrated the effect of the energy dissipation mechanisms enabled in this novel 3D graphene nanolattice on resisting crack propagation. As shown in Fig. 7, MD simulation of a uniaxial tension test in a slab of the graphene nanolattice 200 nm in length and 100 nm in height with a 50 nm edge crack was performed (Movie M6).[8] Unlike the uniform loading in previous uniaxial tension tests, high stress concentration is expected around the crack tip region to promote crack propagation [15]. However, in the graphene nanolattice, it is observed that unit cells near the crack tip transform from the folded state into the extended state first. Correspondingly, the stress near the crack tip region is mostly released and the crack tip is trapped (Fig. 7(*c*)). As the transformation region expands through the lattice, the overall stress level also decreases (Fig. 7(*b*)) due to the reconfiguration of the nanolattice. This example demonstrates that the graphene nanolattice with snap-through instability can tolerate crack-like flaws and behave in a ductile manner within the pseudoplastic deformation region.

Conclusions

Carbon nanolattices have demonstrated great potential in achieving outstanding mechanical performances, including a combination of high strength, low density, good flaw tolerance, and extensive deformability, which are rarely seen in conventional materials. In the present study, we have investigated a type of 3D graphene nanolattice for better ductility through an efficient energy dissipation mechanism design. Specifically, snap-through instability is implemented in the unit cell level via a straw-like graphene cell. With simple lattice architectures, 1D and 3D graphene nanolattices made of such unit cells demonstrate multiple stress-free equilibrium configurations and are elastically reconfigurable. Through tension and compression tests in MD, stress plateaus with saw-teeth-like oscillations and finite hysteresis loops emerge as the number of unit cells in the lattice increases. This lattice-level deformation behavior is explained by a theoretical model of a 1D bi-stable element chain. The theoretical model identifies multiple stable deformation paths available to the lattice. It is the discontinuity and overlapping of these deformation paths that give birth to a pseudoplastic deformation. Interestingly, the theoretical model predicts that the pseudoplastic behavior of the nanolattice is bounded by the deformation behavior of the unit cell. Benefiting from the outstanding property of the nanoscale unit cell, nanolattices with large numbers of such unit cells are predicted to achieve a specific energy dissipation of 233 kJ/kg during a full loading cycle without any irreversible damage, which is one order of magnitude larger than the energy absorbed by carbon steel at failure (16.6 kJ/kg). With such efficient energy dissipation mechanisms enabled by snap-through instability, the graphene nanolattice is demonstrated to be able to trap and postpone crack propagation in MD, showing good tolerance of crack-like flaws and enhanced ductility. This novel capability may broaden the potential application of 3D graphene nanolattices in energy absorption [26] and programmable materials [61].

Funding Data

The authors acknowledge the support the National Science Foundation (NSF) under the (Grant No. CMMI-1634492; Funder ID: 10.13039/501100008982).

Appendix

MD Simulations. MD simulations of graphene nanolattices were carried out via large-scale atomic/molecular massively parallel simulator (LAMMPS) [62]. Visualization was processed via software package OVITO [63]. The interatomic forces were described by the adaptive intermolecular reactive empirical bond order (AIREBO) potential [64]. To avoid a nonphysical post-hardening behavior known to exist for the AIREBO potential, the smaller cutoff distance in the switching function of AIREBO was taken to be 2.0 Å, as suggested by previous studies [14,48,65].

List of Movies of MD Simulations[9]

M1. Uniaxial tension test of a SCNT nanolattice with three unit cells.
M2. Uniaxial tension test of a 3D graphene nanolattice with 3-by-3-by-3 unit cells.
M3. Uniaxial compression test of a 3D graphene nanolattice with 3-by-3-by-3 unit cells.
M4. Uniaxial tension test of a 3D graphene nanolattice with 3-by-3-by-10 unit cells.
M5. Uniaxial compression test of a 3D graphene nanolattice with 3-by-3-by-10 unit cells.
M6. Uniaxial tension test of a graphene nanolattice slab with an edge crack.

References

[1] Bauer, J., Meza, L. R., Schaedler, T. A., Schwaiger, R., Zheng, X., and Valdevit, L., 2017, "Nanolattices: An Emerging Class of Mechanical Metamaterials," Adv. Mater., **29**(40), p. 1701850.
[2] Bauer, J., Schroer, A., Schwaiger, R., and Kraft, O., 2016, "Approaching Theoretical Strength in Glassy Carbon Nanolattices," Nat. Mater., **15**(4), p. 438–443.
[3] Zhang, X., Vyatskikh, A., Gao, H., Greer, J. R., and Li, X., 2019, "Lightweight, Flaw-Tolerant, and Ultrastrong Nanoarchitected Carbon," Proc. Natl. Acad. Sci. U. S. A., **116**(14), pp. 6665–6672.
[4] Qin, Z., Jung, G. S., Kang, M. J., and Buehler, M. J., 2017, "The Mechanics and Design of a Lightweight Three-Dimensional Graphene Assembly," Science Adv., **3**(1), p. e1601536.
[5] Jung, G. S., and Buehler, M. J., 2018, "Multiscale Mechanics of Triply Periodic Minimal Surfaces of Three-Dimensional Graphene Foams," Nano Lett., **18**(8), pp. 4845–4853.
[6] Zhang, X., Zhong, L., Mateos, A., Kudo, A., Vyatskikh, A., Gao, H., Greer, J. R., and Li, X., 2019, "Theoretical Strength and Rubber-Like Behaviour in Micro-Sized Pyrolytic Carbon," Nat. Nanotechnol., **14**(8), pp. 762–769.
[7] Kashani, H., Ito, Y., Han, J., Liu, P., and Chen, M., 2019, "Extraordinary Tensile Strength and Ductility of Scalable Nanoporous Graphene," Sci. Adv., **5**(2), p. eaat6951.
[8] Hu, M., He, J., Zhao, Z., Strobel, T. A., Hu, W., Yu, D., Sun, H., Liu, L., Li, Z., and Ma, M., 2017, "Compressed Glassy Carbon: An Ultrastrong and Elastic Interpenetrating Graphene Network," Sci. Adv., **3**(6), p. e1603213.
[9] Gao, H., Ji, B., Jäger, I. L., Arzt, E., and Fratzl, P., 2003, "Materials Become Insensitive to Flaws at Nanoscale: Lessons From Nature," Proc. Natl. Acad. Sci. U.S.A., **100**(10), pp. 5597–5600.
[10] Gao, H., and Chen, S., 2005, "Flaw Tolerance in a Thin Strip Under Tension," ASME J. Appl. Mech., **72**(5), pp. 732–737.
[11] Gu, X. W., Jafary-Zadeh, M., Chen, D. Z., Wu, Z., Zhang, Y.-W., Srolovitz, D. J., and Greer, J. R., 2014, "Mechanisms of Failure in Nanoscale Metallic Glass," Nano Lett., **14**(10), pp. 5858–5864.
[12] Allen, M. J., Tung, V. C., and Kaner, R. B., 2009, "Honeycomb Carbon: A Review of Graphene," Chem. Rev., **110**(1), pp. 132–145.
[13] Lee, C., Wei, X., Kysar, J. W., and Hone, J., 2008, "Measurement of the Elastic Properties and Intrinsic Strength of Monolayer Graphene," Science, **321**(5887), pp. 385–388.
[14] Zhang, P., Ma, L., Fan, F., Zeng, Z., Peng, C., Loya, P. E., Liu, Z., Gong, Y., Zhang, J., and Zhang, X., 2014, "Fracture Toughness of Graphene," Nat. Commun., **5**, p. 3782.
[15] Anderson, T. L., and Anderson, T. L., 2005, *Fracture Mechanics: Fundamentals and Applications*, CRC Press, Boca Raton, FL.
[16] Schaedler, T. A., Jacobsen, A. J., Torrents, A., Sorensen, A. E., Lian, J., Greer, J. R., Valdevit, L., and Carter, W. B., 2011, "Ultralight Metallic Microlattices," Science, **334**(6058), pp. 962–965.
[17] Meza, L. R., Das, S., and Greer, J. R., 2014, "Strong, Lightweight, and Recoverable Three-Dimensional Ceramic Nanolattices," Science, **345**(6202), pp. 1322–1326.

[8]See Note 3.

[9]See Note 3.

[18] Meza, L. R., Zelhofer, A. J., Clarke, N., Mateos, A. J., Kochmann, D. M., and Greer, J. R., 2015, "Resilient 3D Hierarchical Architected Metamaterials," Proc. Natl. Acad. Sci. U.S.A., **112**(37), pp. 11,502–11,507.
[19] Salari-Sharif, L., Schaedler, T. A., and Valdevit, L., 2014, "Energy Dissipation Mechanisms in Hollow Metallic Microlattices," J. Mater. Res., **29**(16), pp. 1755–1770.
[20] Holmes, D. P., 2019, "Elasticity and Stability of Shape Changing Structures," Curr. Opin. Colloid Interface Sci, **40**, pp. 118–137.
[21] Bertoldi, K., Vitelli, V., Christensen, J., and van Hecke, M., 2017, "Flexible Mechanical Metamaterials," Nat. Rev. Mater., **2**(11), p. 17066.
[22] Fargette, A., Neukirch, S., and Antkowiak, A., 2014, "Elastocapillary Snapping: Capillarity Induces Snap-Through Instabilities in Small Elastic Beams," Phys. Rev. Lett., **112**(13), p. 137802.
[23] Cedolin, L., 2010, *Stability of Structures: Elastic, Inelastic, Fracture and Damage Theories*, World Scientific, Singapore.
[24] Pandey, A., Moulton, D. E., Vella, D., and Holmes, D. P., 2014, "Dynamics of Snapping Beams and Jumping Poppers," Europhys. Lett., **105**(2), p. 24001.
[25] Haghpanah, B., Salari-Sharif, L., Pourrajab, P., Hopkins, J., and Valdevit, L., 2016, "Multistable Shape-Reconfigurable Architected Materials," Adv. Mater., **28**(36), pp. 7915–7920.
[26] Shan, S., Kang, S. H., Raney, J. R., Wang, P., Fang, L., Candido, F., Lewis, J. A., and Bertoldi, K., 2015, "Multistable Architected Materials for Trapping Elastic Strain Energy," Adv. Mater., **27**(29), pp. 4296–4301.
[27] Restrepo, D., Mankame, N. D., and Zavattieri, P. D., 2015, "Phase Transforming Cellular Materials," Extreme Mech. Lett., **4**, pp. 52–60.
[28] Rafsanjani, A., Akbarzadeh, A., and Pasini, D., 2015, "Snapping Mechanical Metamaterials Under Tension," Adv. Mater., **27**(39), pp. 5931–5935.
[29] Li, T., and Zhang, Z., 2010, "Snap-Through Instability of Graphene on Substrates," Nanoscale Res. Lett., **5**(1), p. 169–173.
[30] Puglisi, G., and Truskinovsky, L., 2000, "Mechanics of a Discrete Chain With bi-Stable Elements," J. Mech. Phys. Solids, **48**(1), pp. 1–27.
[31] Puglisi, G., and Truskinovsky, L., 2002, "A Mechanism of Transformational Plasticity," Continuum Mech. Thermodyn., **14**(5), pp. 437–457.
[32] Puglisi, G., and Truskinovsky, L., 2002, "Rate Independent Hysteresis in a Bi-stable Chain," J. Mech. Phys. Solids, **50**(2), pp. 165–187.
[33] Puglisi, G., and Truskinovsky, L., 2005, "Thermodynamics of Rate-Independent Plasticity," J. Mech. Phys. Solids, **53**(3), pp. 655–679.
[34] Williams, P. M., Fowler, S. B., Best, R. B., Toca-Herrera, J. L., Scott, K. A., Steward, A., and Clarke, J., 2003, "Hidden Complexity in the Mechanical Properties of Titin ," Nature, **422**(6930), p. 446.
[35] Oberhauser, A. F., Hansma, P. K., Carrion-Vazquez, M., and Fernandez, J. M., 2001, "Stepwise Unfolding of Titin Under Force-Clamp Atomic Force Microscopy," Proc. Natl. Acad. Sci. U.S.A., **98**(2), pp. 468–472.
[36] Bhattacharya, K., 2003, *Microstructure of Martensite: Why It Forms and How It Gives Rise to the Shape-Memory Effect*, Oxford University Press, Oxford.
[37] Gandhi, M. V., and Thompson, B., 1992, *Smart Materials and Structures*, 1st ed., Springer Science & Business Media, London.
[38] Calladine, C. R., 1989, *Theory of Shell Structures*, Cambridge University Press, Cambridge.
[39] Holmes, D. P., and Crosby, A. J., 2007, "Snapping Surfaces," Adv. Mater., **19**(21), pp. 3589–3593.
[40] Tavakol, B., Bozlar, M., Punckt, C., Froehlicher, G., Stone, H. A., Aksay, I. A., and Holmes, D. P., 2014, "Buckling of Dielectric Elastomeric Plates for Soft, Electrically Active Microfluidic Pumps," Soft Matter, **10**(27), pp. 4789–4794.
[41] Taffetani, M., Jiang, X., Holmes, D. P., and Vella, D., 2018, "Static Bistability of Spherical Caps," Proc. R. Soc. A Math. Phys. Eng. Sci., **474**(2213), p. 20170910.
[42] Panter, J. R., Chen, J., Zhang, T., and Kusumaatmaja, H., 2019, "Harnessing Energy Landscape Exploration to Control the Buckling of Cylindrical Shells," Commun. Phys., **2**(1), pp. 1–9.
[43] Friedman, J. B., 1951, "Flexible Drinking Straw," Google Patents.
[44] Harp, H. J., Leible, W. T., and Mccort, W. M., 1968, "Flexible Drinking Tube," Google Patents.
[45] Bende, N. P., Yu, T., Corbin, N. A., Dias, M. A., Santangelo, C. D., Hanna, J. A., and Hayward, R. C., 2018, "Overcurvature Induced Multistability of Linked Conical Frusta: How a 'Bendy Straw' Holds Its Shape," Soft Matter, **14**(42), pp. 8636–8642.
[46] Ni, B., Zhang, T., Li, J., Li, X., and Gao, H., 2019, *Handbook of Graphene: Physics, Chemistry, and Biology*, 1st ed., T. Stauber, ed., Vol. 2, Wiley, Hoboken, NJ, pp. 1–44.
[47] Zhang, T., Li, X., and Gao, H., 2014, "Defects Controlled Wrinkling and Topological Design in Graphene," J. Mech. Phys. Solids, **67**, pp. 2–13.
[48] Zhang, T., Li, X., and Gao, H., 2014, "Designing Graphene Structures With Controlled Distributions of Topological Defects: A Case Study of Toughness Enhancement in Graphene Ruga," Extreme Mech. Lett., **1**, pp. 3–8.
[49] Li, J., Ni, B., Zhang, T., and Gao, H., 2018, "Phase Field Crystal Modeling of Grain Boundary Structures and Growth in Polycrystalline Graphene," J. Mech. Phys. Solids, **120**, pp. 36–48.
[50] Elder, K. R., Provatas, N., Berry, J., Stefanovic, P., and Grant, M., 2007, "Phase-Field Crystal Modeling and Classical Density Functional Theory of Freezing," Phys. Rev. B, **75**(6), p. 064107.
[51] Seymour, M., and Provatas, N., 2016, "Structural Phase Field Crystal Approach for Modeling Graphene and Other Two-Dimensional Structures," Phys. Rev. B, **93**(3), p. 035447.
[52] Hoover, W. G., 1985, "Canonical Dynamics: Equilibrium Phase-Space Distributions," Phys. Rev. A, **31**(3), p. 1695–1697.
[53] Yazyev, O. V., and Louie, S. G., 2010, "Topological Defects in Graphene: Dislocations and Grain Boundaries," Phys. Rev. B, **81**(19), p. 195420.
[54] Filleter, T., McChesney, J. L., Bostwick, A., Rotenberg, E., Emtsev, K. V., Seyller, T., Horn, K., and Bennewitz, R., 2009, "Friction and Dissipation in Epitaxial Graphene Films," Phys. Rev. Lett., **102**(8), p. 086102.
[55] Rogers, R. C., and Truskinovsky, L., 1997, "Discretization and Hysteresis," Phys. B, **233**(4), pp. 370–375.
[56] Benichou, I., and Givli, S., 2011, "The Hidden Ingenuity in Titin Structure," Appl. Phys. Lett., **98**(9), p. 091904.
[57] Rief, M., Gautel, M., Oesterhelt, F., Fernandez, J. M., and Gaub, H. E., 1997, "Reversible Unfolding of Individual Titin Immunoglobulin Domains by AFM," Science, **276**(5315), pp. 1109–1112.
[58] Fraternali, F., Blesgen, T., Amendola, A., and Daraio, C., 2011, "Multiscale Mass-Spring Models of Carbon Nanotube Foams," J. Mech. Phys. Solids, **59**(1), pp. 89–102.
[59] Benichou, I., and Givli, S., 2013, "Structures Undergoing Discrete Phase Transformation," J. Mech. Phys. Solids, **61**(1), pp. 94–113.
[60] Wei, Y., Wang, B., Wu, J., Yang, R., and Dunn, M. L., 2012, "Bending Rigidity and Gaussian Bending Stiffness of Single-Layered Graphene," Nano Lett., **13**(1), pp. 26–30.
[61] Florijn, B., Coulais, C., and van Hecke, M., 2014, "Programmable Mechanical Metamaterials," Phys. Rev. Lett., **113**(17), p. 175503.
[62] Plimpton, S., 1995, "Fast Parallel Algorithms for Short-Range Molecular Dynamics," J. Comput. Phys., **117**(1), pp. 1–19.
[63] Stukowski, A., 2009, "Visualization and Analysis of Atomistic Simulation Data With OVITO—the Open Visualization Tool," Modell. Simul. Mater. Sci. Eng., **18**(1), p. 015012.
[64] Stuart, S. J., Tutein, A. B., and Harrison, J. A., 2000, "A Reactive Potential for Hydrocarbons With Intermolecular Interactions," J. Chem. Phys., **112**(14), pp. 6472–6486.
[65] Terdalkar, S. S., Huang, S., Yuan, H., Rencis, J. J., Zhu, T., and Zhang, S., 2010, "Nanoscale Fracture in Graphene," Chem. Phys. Lett., **494**(4–6), pp. 218–222.